

IMPLICIT INTEGRATION OF THE TIME-DEPENDENT GINZBURG–LANDAU EQUATIONS OF SUPERCONDUCTIVITY

D. O. GUNTER , H. G. KAPER , AND G. K. LEAF*

Abstract. This article is concerned with the integration of the time-dependent Ginzburg–Landau (TDGL) equations of superconductivity. Four algorithms, ranging from fully explicit to fully implicit, are presented and evaluated for stability, accuracy, and compute time. The benchmark problem for the evaluation is the equilibration of a vortex configuration in a superconductor that is embedded in a thin insulator and subject to an applied magnetic field.

Key words. Time-dependent Ginzburg–Landau equations, superconductivity, vortex solution, implicit time integration

AMS subject classifications. 65M12, 82D55 (Primary); 35K55 (Secondary)

1. Introduction. At the macroscopic level, the state of a superconductor can be described in terms of a complex-valued order parameter and a real vector potential. These variables, which determine the superconducting and electromagnetic properties of the system at equilibrium, are found as solutions of the Ginzburg–Landau (GL) equations of superconductivity. Because they correspond to critical points of the GL energy functional [1, 2], they can, at least in principle, be determined by minimizing a functional. In practice, one introduces a time-like variable and computes equilibrium states by integrating the time-dependent Ginzburg–Landau (TDGL) equations. The TDGL equations, first formulated by Schmid [3] and subsequently derived from microscopic principles by Gor’kov and Éliashberg [4], are nontrivial generalizations of the (time-independent) GL equations, as the time rate of change must be introduced in such a manner that gauge invariance is preserved at all times. The TDGL equations have been analyzed by several authors; see, for example, the articles [5, 6] and the references cited there.

We are interested, in particular, in vortex solutions of the GL equations. These are singular solutions, where the phase of the order parameter changes by 2π along any closed contour surrounding a vortex point. Vortices are of critical importance in technological applications of superconductivity.

Computing vortex solutions of the GL equations by integrating the TDGL equations to equilibrium has the advantage that the solutions thus found are stable. At the same time, one obtains information about the transient behavior of the system. Integrating the TDGL equations to equilibrium is, however, a time-consuming process requiring considerable computing resources. In simulations of vortex dynamics in superconductors, which were performed on an IBM SP with tens of processors in parallel, using a simple one-step Euler integration procedure, we routinely experienced equilibration times on the order of one hundred hours [7, 8, 9]. Incremental changes would gradually drive the system to lower energy levels. These very long equilibration times arise, of course, because we are dealing with large physical systems undergoing a phase transition. The energy landscape for such systems is a broad, gently undulating plain with many shallow local minima. It is therefore important to develop efficient integration techniques that remain stable and accurate as the time step increases.

*Mathematics and Computer Science Division, Argonne National Laboratory, Argonne, IL 60439 (authorname@mcs.anl.gov). This work was supported by the Mathematical, Information, and Computational Sciences Division subprogram of Advanced Scientific Computing Research, U.S. Department of Energy, under Contract W-31-109-Eng-38.

In this article we present four integration techniques ranging from fully explicit to fully implicit for problems on rectangular domains in two dimensions. These two-dimensional domains should be viewed as cross sections of three-dimensional systems that are infinite and homogeneous in the direction of the magnetic field, which is orthogonal to the plane of the cross section. The algorithms are scalable in a multi-processing environment and generalize to three dimensions. We evaluate the performance of each algorithm on the same benchmark problem, namely, the equilibration of a vortex configuration in a system consisting of a superconducting core embedded in a blanket of insulating material (air) and undergoing a transition from the Meissner state to the vortex state under the influence of an externally applied magnetic field. We determine the maximum allowable time step for stability, the number of time steps needed to reach the equilibrium configuration, and the CPU cost per time step.

Different algorithms correspond to different dynamics through state space, so the eventual equilibrium vortex configuration may differ from one algorithm to another. Hence, once we have the equilibrium configurations, we need some measure to assess their accuracy. For this purpose we use three parameters: the number of vortices, the mean intervortex distance (bond length), and the mean bond angle taken over nearest-neighbor pairs of bonds. When each of these parameters differs less than a specified tolerance, we say that the corresponding vortex configurations are the same.

Our investigations show that one can increase the time step by almost two orders of magnitude, without losing stability, by going from the fully explicit to the fully implicit algorithm. The fully implicit algorithm has a higher cost per time step, but the wall clock time needed to compute the equilibrium solution (the most important measure for practical purposes) is still significantly less. The wall clock time can be reduced further by using a multi-timestepping procedure.

In §2, we present the Ginzburg–Landau model of superconductivity, first in its formulation as a system of partial differential equations, then as a system of ordinary differential equations after the spatial derivatives have been approximated by finite differences. In §3, we give four algorithms to integrate the system of ordinary equations: a fully explicit, a semi-implicit, an implicit, and a fully implicit algorithm. In §4, we present and evaluate the results of the investigation. In §5, we further evaluate the fully implicit algorithm from the point of view of parallelism and multi-timestepping. The conclusions are summarized in §6.

2. Ginzburg–Landau Model. The time-dependent Ginzburg–Landau (TDGL) equations of superconductivity [2, 3, 4] are two coupled partial differential equations for the complex-valued *order parameter* $\psi = |\psi|e^{i\phi}$ and the real vector-valued *vector potential* \mathbf{A} ,

$$(2.1) \quad \frac{\hbar^2}{2m_s D} \left(\frac{\partial}{\partial t} + \frac{ie_s}{\hbar} \Phi \right) \psi = -\frac{1}{2m_s} \left(\frac{\hbar}{i} \nabla - \frac{e_s}{c} \mathbf{A} \right)^2 \psi + a\psi - b|\psi|^2\psi,$$

$$(2.2) \quad \nu \left(\frac{1}{c} \frac{\partial \mathbf{A}}{\partial t} + \nabla \Phi \right) = -\frac{c}{4\pi} \nabla \times \nabla \times \mathbf{A} + \mathbf{J}_s.$$

Here, \mathbf{J}_s is the *supercurrent density*, which is a nonlinear function of ψ and \mathbf{A} ,

$$(2.3) \quad \mathbf{J}_s = \frac{e_s \hbar}{2im_s} (\psi^* \nabla \psi - \psi \nabla \psi^*) - \frac{e_s^2}{m_s c} |\psi|^2 \mathbf{A} = \frac{e_s}{m_s} |\psi|^2 \left(\hbar \nabla \phi - \frac{e_s}{c} \mathbf{A} \right).$$

The real scalar-valued *electric potential* Φ is a diagnostic variable. The constants in the equations are \hbar , Planck's constant divided by 2π ; a and b , two positive constants;

c , the speed of light; m_s and e_s , the effective mass and charge, respectively, of the superconducting charge carriers (Cooper pairs); ν , the electrical conductivity; and D , the diffusion coefficient. As usual, i is the imaginary unit, and $*$ denotes complex conjugation.

The quantity $|\psi|^2$ represents the local density of Cooper pairs. The local time rate of change $\partial_t \mathbf{A}$ of \mathbf{A} determines the *electric field*, $\mathbf{E} = (1/c)\partial_t \mathbf{A} + \nabla\Phi$, its spatial variation the (induced) *magnetic field*, $\mathbf{B} = \nabla \times \mathbf{A}$.

The TDGL equations describe the gradient flow for the Ginzburg–Landau energy functional. This functional is zero in the normal state, when $\psi = 0$ and the externally applied magnetic field penetrates the superconductor everywhere, $\nabla \times \mathbf{A} = \mathbf{H}$. In the superconducting state, it is given by the expression

$$(2.4) \quad E = \int \left[\frac{1}{2m_s} \left| \left(\frac{\hbar}{i} \nabla - \frac{e_s}{c} \mathbf{A} \right) \psi \right|^2 + \left(-a|\psi|^2 + \frac{b}{2}|\psi|^4 \right) + |\nabla \times \mathbf{A} - \mathbf{H}|^2 \right] dx.$$

The three terms represent the kinetic energy, the condensation energy, and the field energy, respectively. A thermodynamic equilibrium configuration corresponds to a critical point of E .

The energy functional (2.4) assumes that there are no defects in the superconductor. Material defects can be naturally present or artificially induced and can be in the form of point, planar, or columnar defects (quenched disorder). A material defect results in a local reduction of the depth of the well of the condensation energy. A simple way to include material defects in the Ginzburg–Landau model is by assuming that the parameter a depends on position and has a smaller value wherever a defect is present.

2.1. Dimensionless Form. Let $\psi_\infty^2 = a/b$, and let λ , ξ , and H_c denote the London penetration depth, the coherence length, and the thermodynamic critical field, respectively,

$$(2.5) \quad \lambda = \left(\frac{m_s c^2}{4\pi \psi_\infty^2 e_s^2} \right)^{1/2}, \quad \xi = \left(\frac{\hbar^2}{2m_s a} \right)^{1/2}, \quad H_c = (4\pi a \psi_\infty^2)^{1/2}.$$

In this study, we render the TDGL equations dimensionless by measuring lengths in units of ξ , time in units of the relaxation time ξ^2/D , fields in units of $H_c\sqrt{2}$, and energy densities in units of $(1/4\pi)H_c^2$. The nondimensional TDGL equations are

$$(2.6) \quad \left(\frac{\partial}{\partial t} + i\Phi \right) \psi = \left(\nabla - \frac{i}{\kappa} \mathbf{A} \right)^2 \psi + \tau \psi - |\psi|^2 \psi,$$

$$(2.7) \quad \sigma \left(\frac{\partial \mathbf{A}}{\partial t} + \kappa \nabla \Phi \right) = -\nabla \times \nabla \times \mathbf{A} + \mathbf{J}_s,$$

where

$$(2.8) \quad \mathbf{J}_s = \frac{1}{2i\kappa} (\psi^* \nabla \psi - \psi \nabla \psi^*) - \frac{1}{\kappa^2} |\psi|^2 \mathbf{A} = \frac{1}{\kappa} |\psi|^2 \left(\nabla \phi - \frac{1}{\kappa} \mathbf{A} \right).$$

Here, $\kappa = \lambda/\xi$ is the Ginzburg–Landau parameter and σ is a dimensionless resistivity, $\sigma = (4\pi D/c^2)\nu$. The coefficient τ has been inserted to account for defects; $\tau(x) < 1$ if x is in a defective region; otherwise $\tau(x) = 1$. The nondimensional TDGL equations are associated with the dimensionless energy functional

$$(2.9) \quad E = \int \left[\left| \left(\nabla - \frac{i}{\kappa} \mathbf{A} \right) \psi \right|^2 + \left(-\tau |\psi|^2 + \frac{1}{2} |\psi|^4 \right) + |\nabla \times \mathbf{A} - \mathbf{H}|^2 \right] dx.$$

2.2. Gauge Choice. The (nondimensional) TDGL equations are invariant under a gauge transformation,

$$(2.10) \quad \mathcal{G}_\chi : (\psi, \mathbf{A}, \Phi) \mapsto (\psi e^{i\chi}, \mathbf{A} + \kappa \nabla \chi, \Phi - \partial_t \chi).$$

Here, χ can be any real scalar-valued function of position and time. We maintain the zero-electric potential gauge, $\Phi = 0$, at all times, using the *link variable* \mathbf{U} ,

$$(2.11) \quad \mathbf{U} = \exp \left(-\frac{i}{\kappa} \int \mathbf{A} \right).$$

This definition is componentwise: $U_x = \exp(-i\kappa^{-1} \int^x A_x(x', y, z) dx')$, \dots . The gauged TDGL equations can now be written in the form

$$(2.12) \quad \frac{\partial \psi}{\partial t} = \sum_{\mu=x,y,z} U_\mu^* \frac{\partial^2}{\partial \mu^2} (U_\mu \psi) + \tau \psi - |\psi|^2 \psi,$$

$$(2.13) \quad \sigma \frac{\partial \mathbf{A}}{\partial t} = -\nabla \times \nabla \times \mathbf{A} + \mathbf{J}_s,$$

where

$$(2.14) \quad J_{s,\mu} = \frac{1}{\kappa} \text{Im} \left[(U_\mu \psi)^* \frac{\partial}{\partial \mu} (U_\mu \psi) \right], \quad \mu = x, y, z.$$

2.3. Two-Dimensional Problems. From here on we restrict the discussion to problems on a two-dimensional rectangular domain (coordinates x and y), assuming boundedness in the x direction and periodicity in the y direction. The domain represents a superconducting core surrounded by a blanket of insulating material (air) or a normal metal. The order parameter vanishes outside the superconductor, and no superconducting charge carriers leave the superconductor. The whole system is driven by a time-independent externally applied magnetic field \mathbf{H} that is parallel to the z axis, $\mathbf{H} = (0, 0, H)$. The vector potential and the supercurrent have two nonzero components, $\mathbf{A} = (A_x, A_y, 0)$ and $\mathbf{J}_s = (J_x, J_y, 0)$, while the magnetic field has only one nonzero component, $\mathbf{B} = (0, 0, B)$, where $B = \partial_x A_y - \partial_y A_x$.

2.4. Spatial Discretization. The physical configuration to be modeled (superconductor embedded in blanket material) is periodic in y and bounded in x . In the x direction, we distinguish three subdomains: an interior subdomain occupied by the superconducting material and two subdomains, one on either side, occupied by the blanket material. We take the two blanket layers to be equally thick, but do not assume that the problem is symmetric around the midplane. (Possible sources of asymmetry are material defects in the system, surface currents, and different field strengths on the two outer surfaces.)

We impose a regular grid with mesh widths h_x and h_y ,

$$(2.15) \quad \Omega_{i,j} = (x_i, x_{i+1}) \times (y_j, y_{j+1}), \quad x_i = x_0 + ih_x; \quad y_j = y_0 + jh_y,$$

assuming the following correspondences:

$$\begin{aligned} \text{Left outer surface:} & \quad x = x_0 + \frac{1}{2}h_x, & \quad i = 0, \\ \text{Left interface:} & \quad x = x_{n_{sx}-1} + \frac{1}{2}h_x, & \quad i = n_{sx} - 1, \\ \text{Right interface:} & \quad x = x_{n_{ex}} + \frac{1}{2}h_x, & \quad i = n_{ex}, \\ \text{Right outer surface:} & \quad x = x_{n_x} + \frac{1}{2}h_x, & \quad i = n_x. \end{aligned}$$

One period in the y direction is covered by the points $j = 1, \dots, n_y$. We use the symbols Sc and Bl to denote the index sets for the superconducting and blanket region, respectively,

$$(2.16) \quad \text{Sc} = \{(i, j) : (i, j) \in [n_{sx}, n_{ex}] \times [1, n_y]\},$$

$$(2.17) \quad \text{Bl} = \{(i, j) : (i, j) \in [1, n_{sx} - 1] \cup [n_{ex} + 1, n_x] \times [1, n_y]\}.$$

The order parameter ψ is evaluated at the grid vertices,

$$(2.18) \quad \psi_{i,j} = \psi(x_i, y_j), \quad (i, j) \in \text{Sc},$$

the components A_x and A_y of the vector potential at the midpoints of the respective edges,

$$(2.19) \quad A_{x;i,j} = A_x(x_i + \frac{1}{2}h_x, y_j), \quad A_{y;i,j} = A_y(x_i, y_j + \frac{1}{2}h_y), \quad (i, j) \in \text{Sc} \cup \text{Bl},$$

and the induced magnetic field B at the center of a grid cell,

$$(2.20) \quad \begin{aligned} B_{i,j} &= B(x_i + \frac{1}{2}h_x, y_j + \frac{1}{2}h_y) \\ &= \frac{A_{y;i+1,j} - A_{y;i,j}}{h_x} - \frac{A_{x;i,j+1} - A_{x;i,j}}{h_y}, \quad (i, j) \in \text{Sc} \cup \text{Bl}, \end{aligned}$$

see Fig. 2.1. The values of the link variables and the supercurrent are computed from

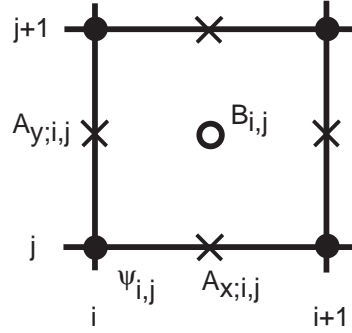


FIG. 2.1. Computational cell with evaluation points for ψ , A_x , and A_y .

the expressions

$$(2.21) \quad U_{x;i,j} = e^{-i\kappa^{-1}h_x A_{x;i,j}}, \quad U_{y;i,j} = e^{-i\kappa^{-1}h_y A_{y;i,j}},$$

$$(2.22) \quad J_{x;i,j} = \frac{1}{\kappa h_x} \text{Im} [\psi_{i,j}^* U_{x;i,j} \psi_{i+1,j}], \quad J_{y;i,j} = \frac{1}{\kappa h_y} \text{Im} [\psi_{i,j}^* U_{y;i,j} \psi_{i,j+1}].$$

The discretized TDGL equations are

$$(2.23) \quad \frac{d\psi_{i,j}}{dt} = (L_{xx}(U_{x;\cdot,j})\psi_{\cdot,j})_i + (L_{yy}(U_{y;i,\cdot})\psi_{i,\cdot})_j + N(\psi_{i,j}), \quad (i, j) \in \text{Sc},$$

$$(2.24) \quad \sigma \frac{dA_{x;i,j}}{dt} = (D_{yy}A_{x;i,\cdot})_j - (D_{yx}A_{y;\cdot,i})_{i,j} + J_{x;i,j}, \quad (i, j) \in \text{Sc} \cup \text{Bl},$$

$$(2.25) \quad \sigma \frac{dA_{y;i,j}}{dt} = (D_{xx}A_{y;\cdot,j})_i - (D_{xy}A_{x;\cdot,i})_{i,j} + J_{y;i,j}. \quad (i, j) \in \text{Sc} \cup \text{Bl},$$

where

$$(2.26) \quad (L_{xx}(U_{x;\cdot,j})\psi_{\cdot,j})_i = h_x^{-2} [U_{x;i,j}\psi_{i+1,j} - 2\psi_{i,j} + U_{x;i-1,j}^*\psi_{i-1,j}],$$

$$(2.27) \quad (L_{yy}(U_{y;i,\cdot})\psi_{i,\cdot})_j = h_y^{-2} [U_{y;i,j}\psi_{i,j+1} - 2\psi_{i,j} + U_{y;i,j-1}^*\psi_{i,j-1}],$$

$$(2.28) \quad N(\psi_{i,j}) = \tau_{i,j}\psi_{i,j} - |\psi_{i,j}|^2\psi_{i,j},$$

$$(2.29) \quad (D_{yy}A_{x;i,\cdot})_j = h_y^{-2} [A_{x;i,j+1} - 2A_{x;i,j} + A_{x;i,j-1}],$$

$$(2.30) \quad (D_{xx}A_{y;\cdot,j})_i = h_x^{-2} [A_{y;i+1,j} - 2A_{y;i,j} + A_{y;i-1,j}],$$

$$(2.31) \quad (D_{yx}A_{y;\cdot,\cdot})_{i,j} = h_x^{-1}h_y^{-1} [(A_{y;i+1,j} - A_{y;i,j}) - (A_{y;i+1,j-1} - A_{y;i,j-1})],$$

$$(2.32) \quad (D_{xy}A_{x;\cdot,\cdot})_{i,j} = h_x^{-1}h_y^{-1} [(A_{x;i,j+1} - A_{x;i,j}) - (A_{x;i-1,j+1} - A_{x;i-1,j})].$$

The interface conditions are

$$(2.33) \quad \psi_{n_{sx}-1,j} = U_{x;n_{sx}-1,j}\psi_{n_{sx},j}, \quad \psi_{n_{ex}+1,j} = U_{x;n_{ex},j}^*\psi_{n_{ex},j}, \quad j = 1, \dots, n_y.$$

At the outer boundary, B is given,

$$(2.34) \quad B_{0,j} = H_{L_j}, \quad B_{n_x,j} = H_{R_j}, \quad j = 1, \dots, n_y.$$

The resulting approximation is second-order accurate [10].

3. Time Integration. We now address the integration of Eqs. (2.23)–(2.25). The first equation, which controls the evolution of ψ , involves the second-order linear finite-difference operators L_{xx} and L_{yy} , whose coefficients depend on A_x and A_y , and the local nonlinear operator N , which involves neither A_x nor A_y . Each of the other two equations, which control the evolution of A_x and A_y respectively, involves likewise a second-order linear finite-difference operator, but with constant coefficients, and the nonlinear supercurrent operator, which involves ψ , A_x , and A_y . The following algorithms are distinguished by whether the various operators are treated explicitly or implicitly.

3.1. Fully Explicit Integration. Algorithm I uses a fully explicit forward Euler time-marching procedure for ψ , A_x , and A_y . Starting from an initial triple (ψ^0, A_x^0, A_y^0) , we solve for $n = 0, 1, \dots$,

$$(3.1) \quad \frac{\psi_{i,j}^{n+1} - \psi_{i,j}^n}{\Delta t} = (L_{xx}(U_{x;\cdot,j}^n)\psi_{\cdot,j}^n)_i + (L_{yy}(U_{y;i,\cdot}^n)\psi_{i,\cdot}^n)_j + N(\psi_{i,j}^n), \quad (i,j) \in \text{Sc},$$

$$(3.2) \quad \sigma \frac{A_{x;i,j}^{n+1} - A_{x;i,j}^n}{\Delta t} = (D_{yy}A_{x;i,\cdot}^n)_j - (D_{yx}A_{y;\cdot,\cdot}^n)_{i,j} + J_{x;i,j}^n, \quad (i,j) \in \text{Sc} \cup \text{Bl},$$

$$(3.3) \quad \sigma \frac{A_{y;i,j}^{n+1} - A_{y;i,j}^n}{\Delta t} = (D_{xx}A_{y;\cdot,j}^n)_i - (D_{xy}A_{x;\cdot,\cdot}^n)_{i,j} + J_{y;i,j}^n. \quad (i,j) \in \text{Sc} \cup \text{Bl},$$

where J^n is defined in terms of ψ^n , A_x^n , and A_y^n in the obvious way. The initial triple is usually chosen so the superconductor is in the Meissner state, with a seed present to trigger the transition to the vortex state.

Algorithm I has been described in [10]. It has been implemented in a distributed-memory multiprocessor environment (IBM SP2); the transformations necessary to achieve the parallelism have been described in [11]. The code uses the Message Passing Interface (MPI) standard [12] as implemented in the MPICH software library [13] for domain decomposition, interprocessor communication, and file I/O. The code has

been used extensively to study vortex dynamics in superconducting media [7, 8, 9]. The underlying algorithm provides highly accurate solutions but requires a significant number of time steps for equilibration. For stability reasons, the time step Δt cannot exceed 0.0025.

3.2. Semi-Implicit Integration. Algorithm II is generated by an implicit treatment of the second-order linear finite-difference operators D_{yy} and D_{xx} in the equations for A_x and A_y , respectively,

$$(3.4) \quad \frac{\psi_{i,j}^{n+1} - \psi_{i,j}^n}{\Delta t} = (L_{xx}(U_{x;\cdot,j}^n)\psi_{i,j}^n)_i + (L_{yy}(U_{y;i,\cdot}^n)\psi_{i,j}^n)_j + N(\psi_{i,j}^n), \quad (i, j) \in \text{Sc},$$

$$(3.5) \quad \sigma \frac{A_{x;i,j}^{n+1} - A_{x;i,j}^n}{\Delta t} = (D_{yy}A_{x;i,\cdot}^{n+1})_j - (D_{yx}A_{y;\cdot,i}^n)_{i,j} + J_{x;i,j}^n, \quad (i, j) \in \text{Sc} \cup \text{Bl},$$

$$(3.6) \quad \sigma \frac{A_{y;i,j}^{n+1} - A_{y;i,j}^n}{\Delta t} = (D_{xx}A_{y;\cdot,j}^{n+1})_i - (D_{xy}A_{x;\cdot,i}^n)_{i,j} + J_{y;i,j}^n. \quad (i, j) \in \text{Sc} \cup \text{Bl}.$$

Equations (3.5) and (3.6) lead to two linear systems of equations,

$$(3.7) \quad \left(I - \frac{\Delta t}{\sigma} D_{yy} \right) A_{x;i}^{n+1} = F_i(\psi^n, A_x^n, A_y^n), \quad i = 1, \dots, n_x - 1,$$

$$(3.8) \quad \left(I - \frac{\Delta t}{\sigma} D_{xx} \right) A_{y;j}^{n+1} = G_j(\psi^n, A_x^n, A_y^n), \quad j = 1, \dots, n_y,$$

for the vectors of unknowns $A_{x;i} = \{A_{x;i,j} : j = 1, \dots, n_y\}$ and $A_{y;j} = \{A_{y;i,j} : i = 1, \dots, n_x - 1\}$. The matrix D_{yy} has dimension $n_y \times n_y$ and is periodic tridiagonal with elements $-h_y^{-2}, 2h_y^{-2}, -h_y^{-2}$; the matrix D_{xx} has dimension $(n_x - 1) \times (n_x - 1)$ and is tridiagonal with elements $-h_x^{-2}, 2h_x^{-2}, -h_x^{-2}$, (except along the edges, because of the boundary conditions). Both matrices are independent of i and j . Furthermore, if the boundary conditions are time independent, they are constant throughout the time-stepping process. Hence, the coefficient matrices in Eqs. (3.7) and (3.8) need to be factored only once; in fact, the factorization can be done in the preprocessing stage and the factors can be stored.

In a parallel processing environment, the coefficient matrices extend over several processors, so Eqs. (3.7) and (3.8) are broken up in blocks corresponding to the manner in which the computational mesh is distributed among the processor set. We first solve the equations within each processor (inner iterations) and then couple the solutions across processor boundaries (outer iterations). Hence, we deal with interprocessor coupling in an iterative fashion. Two to three inner iterations usually suffice to reach a desired tolerance for convergence. After each inner iteration, each processor shares boundary data with its neighbors through MPI calls.

3.3. Implicit Integration. Algorithm III combines the semi-implicit treatment of A_x and A_y with an implicit treatment of the order parameter,

$$(3.9) \quad \frac{\psi_{i,j}^{n+1} - \psi_{i,j}^n}{\Delta t} = (L_{xx}(U_{x;\cdot,j}^n)\psi_{i,j}^{n+1})_i + (L_{yy}(U_{y;i,\cdot}^n)\psi_{i,j}^{n+1})_j + N(\psi_{i,j}^n), \quad (i, j) \in \text{Sc},$$

$$(3.10) \quad \sigma \frac{A_{x;i,j}^{n+1} - A_{x;i,j}^n}{\Delta t} = (D_{yy}A_{x;i,\cdot}^{n+1})_j - (D_{yx}A_{y;\cdot,i}^n)_{i,j} + J_{x;i,j}^n, \quad (i, j) \in \text{Sc} \cup \text{Bl},$$

$$(3.11) \quad \sigma \frac{A_{y;i,j}^{n+1} - A_{y;i,j}^n}{\Delta t} = (D_{xx}A_{y;\cdot,j}^{n+1})_i - (D_{xy}A_{x;\cdot,i}^n)_{i,j} + J_{y;i,j}^n. \quad (i, j) \in \text{Sc} \cup \text{Bl}.$$

The second and third equation are solved as in the semi-implicit algorithm of the preceding section. The first equation is solved by a method similar to the method of Douglas and Gunn [14] for the Laplacian.

We begin by transforming Eq. (3.9) into an equation for the correction matrix $\phi^{n+1} = \psi^{n+1} - \psi^n$. The equation has the general form

$$(3.12) \quad (I - \Delta t(L_{xx} + L_{yy})) \phi^{n+1} = F(\psi^n, A_x^n, A_y^n).$$

If Δt is sufficiently small, we may replace the operator in the left member by an approximate factorization,

$$(3.13) \quad (I - \Delta t(L_{xx} + L_{yy})) \approx (I - \Delta t L_{xx})(I - \Delta t L_{yy}),$$

and consider, instead of Eq. (3.12),

$$(3.14) \quad (I - \Delta t L_{xx})(I - \Delta t L_{yy}) \phi^{n+1} = F(\psi^n, A_x^n, A_y^n).$$

This equation can be solved in two steps,

$$(3.15) \quad (I - \Delta t L_{xx}) \varphi = F,$$

$$(3.16) \quad (I - \Delta t L_{yy}) \phi^{n+1} = \varphi.$$

The conditions (2.33), which must be satisfied at the interface between the superconductor and the blanket material, require some care. If we impose the conditions at every time step, then

$$\begin{aligned} \phi_{n_{sx}-1,j}^{n+1} &= U_{x;n_{sx}-1,j}^{n+1} \phi_{n_{sx},j}^{n+1} + [U_{x;n_{sx}-1,j}^{n+1} - U_{x;n_{sx}-1,j}^n] \psi_{n_{sx},j}^n, \\ \phi_{n_{ex}+1,j}^{n+1} &= (U_{x;n_{ex},j}^{n+1})^* \phi_{n_{ex},j}^{n+1} + [(U_{x;n_{ex},j}^{n+1})^* - (U_{x;n_{ex}-1,j}^n)^*] \psi_{n_{sx},j}^n, \end{aligned}$$

for $j = 1, \dots, n_y$. These conditions couple the correction ϕ to the update of A_x . To eliminate this coupling, we solve Eq. (3.12) subject to the reduced interface conditions

$$(3.17) \quad \phi_{n_{sx}-1,j}^{n+1} = U_{x;n_{sx}-1,j}^{n+1} \phi_{n_{sx},j}^{n+1}, \quad j = 1, \dots, n_y,$$

$$(3.18) \quad \phi_{n_{ex}+1,j}^{n+1} = (U_{x;n_{ex},j}^{n+1})^* \phi_{n_{ex},j}^{n+1}, \quad j = 1, \dots, n_y.$$

When Eq. (3.12) is replaced by Eq. (3.14), these conditions are inherited by the system (3.15).

3.4. Fully Implicit Integration. Algorithm IV uses a fully implicit integration procedure for the order parameter,

$$(3.19) \quad \frac{\psi_{i,j}^{n+1} - \psi_{i,j}^n}{\Delta t} = (L_{xx}(U_{x;.,j}^n) \psi_{i,j}^{n+1})_i + (L_{yy}(U_{y;i, .}^n) \psi_{i,j}^{n+1})_j + N(\psi_{i,j}^{n+1}), \quad (i, j) \in \text{Sc},$$

$$(3.20) \quad \sigma \frac{A_{x;i,j}^{n+1} - A_{x;i,j}^n}{\Delta t} = (D_{yy} A_{x;i, .}^{n+1})_j - (D_{yx} A_{y;., j}^n)_{i,j} + J_{x;i,j}^n, \quad (i, j) \in \text{Sc} \cup \text{Bl},$$

$$(3.21) \quad \sigma \frac{A_{y;i,j}^{n+1} - A_{y;i,j}^n}{\Delta t} = (D_{xx} A_{y;., j}^{n+1})_i - (D_{xy} A_{x;., j}^n)_{i,j} + J_{y;i,j}^n. \quad (i, j) \in \text{Sc} \cup \text{Bl}.$$

The new element here is the term $N(\psi_{i,j}^{n+1})$ in the first equation.

The second and third equations are solved again as in the semi-implicit algorithm. The first equation is solved by a slight modification of the method used in the implicit algorithm of the preceding section, The modification is brought about by the approximation

$$(3.22) \quad N(\psi^{n+1}) = \tau\psi^{n+1} - |\psi^{n+1}|^2\psi^{n+1} \approx \frac{1}{\Delta t} (S(\psi^n) - \psi^n),$$

where S is a nonlinear map,

$$(3.23) \quad S(\psi) = \frac{\tau^{1/2}\psi}{[|\psi|^2 + (\tau - |\psi|^2)\exp(-2\tau\Delta t)]^{1/2}}.$$

(This approximation is explained in the remark below.) Equation (3.19) is again of the form (3.12), but with a different right-hand side,

$$(3.24) \quad (I - \Delta t(L_{xx} + L_{yy}))\phi^{n+1} = G(\psi^n, A_x^n, A_y^n).$$

The difference is that, where F in Eq. (3.12) contains a term $(\Delta t)N(\psi^n)$, G in Eq. (3.24) contains the more complicated term $S(\psi^n) - \psi^n$.

Remark. The approximation (3.22) is suggested by semigroup theory. Symbolically,

$$(3.25) \quad N(\psi) = \lim_{\Delta t \rightarrow 0} \frac{S(\Delta t)\psi - \psi}{\Delta t}.$$

To find an expression for the “semigroup” S , we start from the continuous TDGL equations (2.6)–(2.8) (zero-electric potential gauge, $\Phi = 0$), using the polar representation $\psi = |\psi|e^{i\phi}$,

$$(3.26) \quad \partial_t |\psi| = \Delta |\psi| - |\psi| |\nabla \phi - \kappa^{-1} \mathbf{A}|^2 + \tau |\psi| - |\psi|^3,$$

$$(3.27) \quad |\psi| \partial_t \phi = 2(\nabla |\psi|) \cdot (\nabla \phi - \kappa^{-1} \mathbf{A}) + |\psi| \nabla \cdot (\nabla \phi - \kappa^{-1} \mathbf{A}),$$

$$(3.28) \quad \sigma \partial_t \mathbf{A} = -\nabla \times \nabla \times \mathbf{A} + \kappa^{-1} |\psi|^2 (\nabla \phi - \kappa^{-1} \mathbf{A}).$$

At this point, we are interested in the effect of the nonlinear term $|\psi|^3$ on the dynamics. To highlight this effect, we concentrate on the time evolution of the scalar $u = |\psi|$ and the vector $v = \nabla \phi - \kappa^{-1} \mathbf{A}$. (In physical terms, u^2 is the density of superconducting charge carriers, while $u^2 v$ is κ times the supercurrent density.) Ignoring their spatial variations, we have a dynamical system,

$$(3.29) \quad u' = -u|v|^2 + \tau u - u^3,$$

$$(3.30) \quad v' = -\varepsilon u^2 v,$$

where $'$ denotes differentiation with respect to t , and $\varepsilon = (\kappa^2 \sigma)^{-1}$. This system yields a pair of ordinary differential equations for the scalars $x = u^2$ and $y = |v|^2$,

$$(3.31) \quad x' = 2x(\tau - x - y),$$

$$(3.32) \quad y' = -2\varepsilon xy.$$

If κ is large, ε is small, and the dynamics are readily analyzed. To leading order, y is constant; $y = 0$ is the only meaningful choice. (Recall that $xy^{1/2}$ is κ times the magnitude of the supercurrent density.) Then the dynamics of x are given by

$$(3.33) \quad x' = 2x(\tau - x).$$

We integrate this equation from $t = t_n$ to t ,

$$(3.34) \quad x(t) = \frac{\tau x(t_n)}{x(t_n) + (\tau - x(t_n)) \exp(-2\tau(t - t_n))}.$$

In particular,

$$(3.35) \quad x(t_{n+1}) = \frac{\tau x(t_n)}{x(t_n) + (\tau - x(t_n)) \exp(-2\tau\Delta t)},$$

where $\Delta t = t_{n+1} - t_n$. Since $x(t_n) = |\psi^n|^{1/2}$ and $x(t_{n+1}) = |\psi^{n+1}|^{1/2}$, it follows that

$$(3.36) \quad |\psi^{n+1}| = \frac{\tau^{1/2} |\psi^n|}{[|\psi^n|^2 + (\tau - |\psi^n|^2) \exp(-2\tau\Delta t)]^{1/2}}.$$

The phase ϕ of ψ is constant in time. If we multiply both sides by $e^{i\phi}$, we obtain the expression (3.23) for the “semigroup” S .

4. Evaluation. We now present the results of several experiments, where the algorithms described in the preceding section were applied to a benchmark problem.

4.1. Benchmark Problem. The benchmark problem adopted for this investigation is the equilibration of a vortex configuration in a homogeneous superconductor without defects ($\kappa = 16$, $\sigma = 1$, $\tau = 1$) embedded in a thin insulator (air), where the entire system is periodic in the direction of the free surfaces (y).

The superconductor measures 128ξ in the transverse (x) direction. The thickness of the insulating layer on either side is taken to be 2ξ , so the width of the entire system is 132ξ . The period in the y direction is taken to be 192ξ , so the entire system measures $132\xi \times 192\xi$.

The computational grid is uniform, with a mesh width $h_x = h_y = \frac{1}{2}\xi$. The periodic boundary conditions in the y direction are handled through ghost points, so the computational grid has 264×386 vertices. The index sets for the superconductor and blanket (see Eqs. (2.16) and (2.17)) are

$$(4.1) \quad \text{Sc} = \{(i, j) : i = 5, \dots, 260, j = 1, \dots, 386\},$$

$$(4.2) \quad \text{Bl} = \{(i, j) : i = 1, \dots, 4, 261, \dots, 264, j = 1, \dots, 386\}.$$

The applied field is uniform,

$$(4.3) \quad H_L = H_R = H = 0.5.$$

(Units of H are $H_c\sqrt{2}$, so $H \approx 0.707\dots H_c$). As there is no transport current in the system, the solution of the TDGL equations tends to an equilibrium state.

4.2. Benchmark Solution. First, preliminary runs were made to determine, for each algorithm, the optimal number of processors in a multiprocessing environment. Figure 4.1 shows the wall clock time for 50 time steps against the number of processors on the IBM SP2. Each algorithm shows a saturation around 16 processors, beyond which any improvement becomes marginal. All problems were subsequently run on 16 processors.

Next, we used the fully explicit Algorithm I to establish a benchmark equilibrium configuration. We integrated Eqs. (3.1)–(3.3) with a time step $\Delta t = 0.0025$ (units of ξ^2/D), the maximal value for which the algorithm remained stable, and followed the

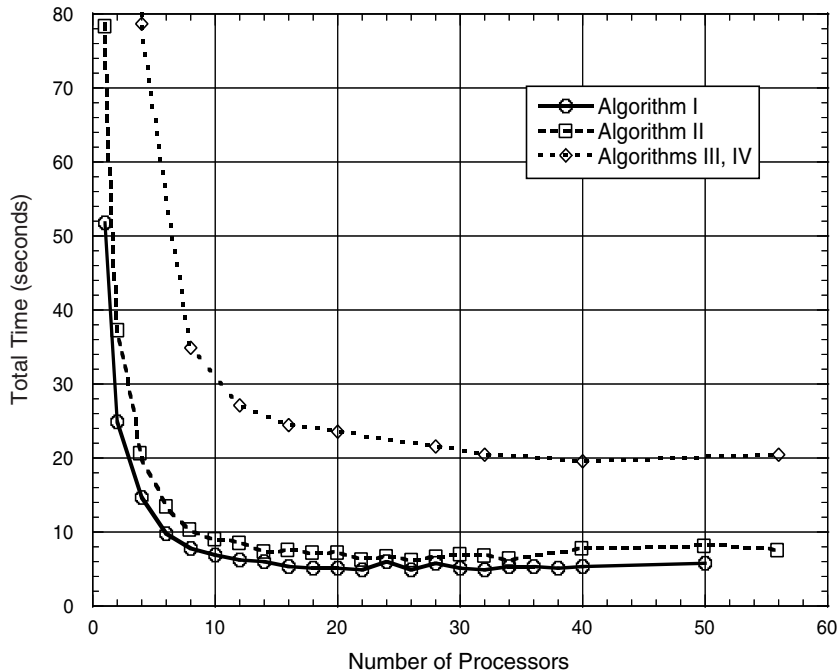


FIG. 4.1. Elapsed time for 50 time steps as a function of the number of processors.

evolution of the vortex configuration by monitoring the number of vortices and their positions. Equilibrium was reached after 10,000,000 time steps, when the number of vortices remained constant and the vortex positions varied less than 1.0×10^{-6} (units of ξ). The equilibrium vortex configuration had 116 vortices arranged in a hexagonal pattern; see Fig. 4.2. The wall clock time for the entire computation was approximately 3,000 minutes. The elapsed time per time step (0.018 seconds) is a measure for the computational cost of Algorithm I.

4.3. Evaluation of Algorithms II–IV. With the benchmark solution in place, we evaluated each of the remaining algorithms (II–IV) for stability, accuracy, and computational cost.

We found the stability limit in the obvious way, gradually increasing the time step and integrating to equilibrium until arithmetic divergences caused the algorithm to fail. Equilibrium was defined by the same criteria as for the benchmark solution: no change in the number of vortices and a variation in the vortex positions of less than 1.0×10^{-6} .

Because each algorithm defines its own path through phase space, one cannot expect to find identical equilibrium configurations nor equilibrium configurations that are exactly the same as the benchmark. The equilibrium vortex configurations for the four algorithms were indeed different, albeit slightly. To measure the differences quantitatively, we computed the following three parameters: (i) the number of vortices in the superconducting region, (ii) the mean bond length joining neighboring pairs of vortices, and (iii) the mean bond angle subtended by neighboring bonds throughout the vortex lattice. In all cases, the number of vortices was the same (116); the mean bond length varied less than $1.0 \times 10^{-3}\xi$, and the mean bond angle varied by less than

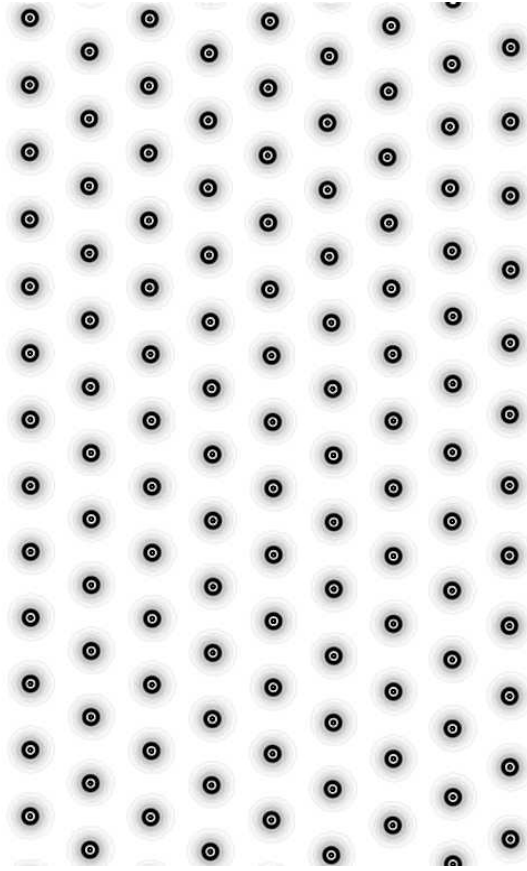


FIG. 4.2. *Equilibrium vortex configuration for the benchmark problem.*

1.0×10^{-3} radians. Within these tolerances, the equilibrium vortex configurations were the same.

The results are given in Table 4.1; Δt is the time step at the stability limit (units

TABLE 4.1
Performance data for Algorithms I-IV.

Algorithm	Δt	N	C	T
I	0.0025	10,000,000	0.018	3,000
II	0.0500	500,000	0.103	858
III	0.1000	250,000	0.232	967
IV	0.1900	100,000	0.233	388

of ξ^2/D), N the number of time steps needed to reach equilibrium, and C the cost of the algorithm (seconds per time step). From these data we obtain the wall clock time needed to compute the equilibrium configuration, $T = NC/60$ (minutes).

Note that the existence of a stability limit for Algorithm IV is a consequence of the implementation in a multiprocessing environment. Since we restrict interprocessor communication to the end of each time step, the fully implicit character of the algorithm is lost. On a single processor, Algorithm IV is fully implicit, and the stability limit is infinite.

5. Further Evaluation of Algorithm IV. We evaluated the fully implicit Algorithm IV in more detail by considering its speedup in a multiprocessing environment and its performance under a multi-timestepping procedure.

5.1. Parallelism. First, we investigated the speedup of Algorithm IV in a multiprocessing environment, using the the benchmark problem and two other problems, obtained from the benchmark problem by twice doubling the size of the system in each direction. The mesh width was kept constant at $\frac{1}{2}\xi$, so the resulting computational grid had 264×386 vertices for the benchmark problem, 528×772 vertices for the intermediate problem, and 1056×1544 vertices for the largest problem. Speedup was defined as the ratio of the wall clock time (exclusive of I/O) to reach equilibrium on p processors divided by the time to reach equilibrium on a single processor for the benchmark and intermediate problem, or twice the time to reach equilibrium on two processors for the largest problem. (The largest problem did not fit on a single processor.) The results are given in Fig. 5.1. The curve for the benchmark problem

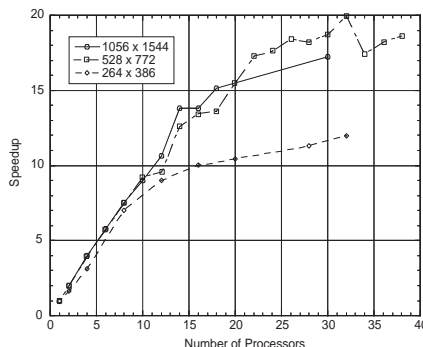


FIG. 5.1. Performance of Algorithm IV in a multiprocessing environment.

was obtained as an average over many runs; the data for the intermediate and largest problem were obtained from single runs, hence they are less smooth. The speedup is clearly linear when the number of processors is small; it becomes sublinear at about 12 processors for the smallest problem, 14 processors for the intermediate problem, and 18 processors for the largest problem.

5.2. Multi-timestepping. The final set of experiments shows that the performance of Algorithm IV is enhanced by a multi-timestepping procedure, where \mathbf{A} is updated less frequently than ψ ,

$$(5.1) \quad \frac{\psi_{i,j}^{n+1} - \psi_{i,j}^n}{\Delta t} = (L_{xx}(U_{x;\cdot,j}^n)\psi_{i,j}^{n+1})_i + (L_{yy}(U_{y;i,\cdot}^n)\psi_{i,\cdot}^{n+1})_j + N(\psi_{i,j}^{n+1}), \quad (i,j) \in \text{Sc},$$

$$(5.2) \quad \sigma \frac{A_{x;i,j}^{n+m} - A_{x;i,j}^n}{m\Delta t} = (D_{yy}A_{x;i,\cdot}^{n+m})_j - (D_{yx}A_{y;\cdot,\cdot}^n)_{i,j} + J_{x;i,j}^n, \quad (i,j) \in \text{Sc} \cup \text{Bl},$$

$$(5.3) \quad \sigma \frac{A_{y;i,j}^{n+m} - A_{y;i,j}^n}{m\Delta t} = (D_{xx}A_{y;\cdot,j}^{n+m})_i - (D_{xy}A_{x;\cdot,\cdot}^n)_{i,j} + J_{y;i,j}^n. \quad (i,j) \in \text{Sc} \cup \text{Bl}.$$

When $m = 1$, both ψ and \mathbf{A} are updated at every time step, but when m is greater than 1, \mathbf{A} is updated only every m th time step. In the limit as $m \rightarrow \infty$, this procedure yields the frozen-field approximation, which is a good approximation of the Ginzburg–Landau model near the upper critical field when the charge of the superconducting charge carriers is small [15].

We applied this modification of Algorithm IV with $m = 10, 15$ to the benchmark problem of §4. The results are given in Table 5.1. All computations were done with

TABLE 5.1
Effect of update frequency on time and cost of Algorithm IV.

m	N	C	T
1	100,000	0.2330	388
10	200,000	0.0707	236
15	250,000	0.0646	270

$\Delta t = 0.19$ (units of ξ^2/D). The data for the computation with $m = 1$ are taken from Table 4.1. We observe that the cost of the algorithm (C , seconds per time step) decreases with increasing m , while the number of time steps to equilibrium (N) increases. If $m = 10$, the overall wall-clock time ($T = NC/60$, minutes) is approximately one-third less than the wall-clock time for $m = 1$. For larger values of m , the increase in the number of steps needed to reach equilibrium offsets any gain from the decrease in cost. These data suggest an optimal strategy, where \mathbf{A} is updated every 10 time steps. Figure 5.2 shows the effect of the updating frequency on the evolution of the free-energy functional (2.9). Note the dramatic increase of the wall-clock time for $m = 15$. Eventually, the curve for $m = 15$ merges with the other curves, but this happens well beyond the range of the figure.

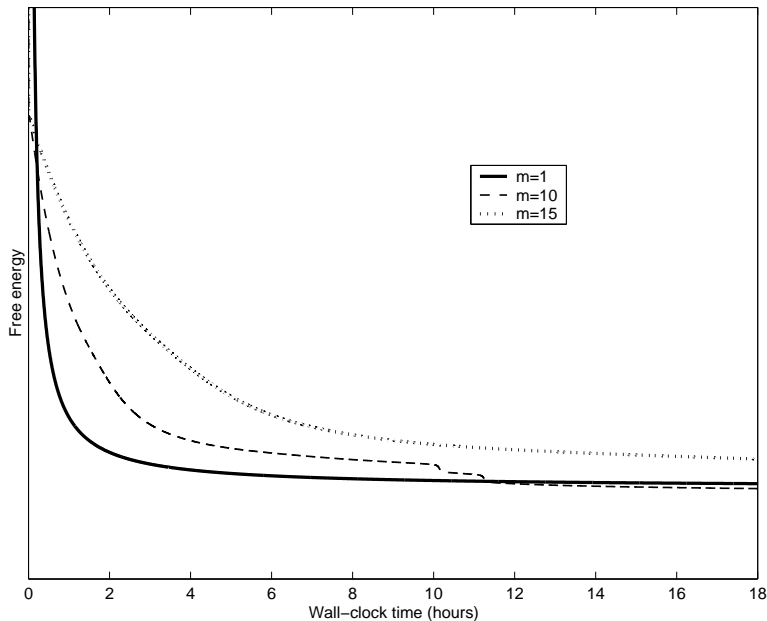


FIG. 5.2. *Effect of the updating frequency on the evolution of the energy functional.*

6. Conclusions. The results of the investigation lead to the following conclusions.

(i) One can increase the time step Δt nearly 80-fold, without losing stability, by going from the fully explicit Algorithm I to the fully implicit Algorithm IV.

(ii) As one goes to the fully implicit Algorithm IV, the complexity of the matrix calculations and, hence, the cost C of a single time step increase.

(iii) The increase in the cost C per time step is more than offset by the increase in the size of the time step Δt . In fact, the wall clock time needed to compute the same equilibrium state with the fully implicit Algorithm IV is one-sixth of the wall clock time for the fully explicit Algorithm I.

(iv) The (physical) time to reach equilibrium—that is, $N\Delta t$, the number of time steps needed to reach equilibrium times the step size—is (approximately) the same for all algorithms, namely, 25,000 (units of ξ^2/D).

(v) The fully implicit Algorithm IV displays linear speedup in a multiprocessing environment. The speedup curves show sublinear behavior when the number of processors is large.

(vi) The performance of the fully implicit Algorithm IV can be improved further by a multi-timestepping procedure, where the vector potential \mathbf{A} is updated less frequently than the order parameter ψ .

REFERENCES

- [1] V. L. GINZBURG AND L. D. LANDAU, On the theory of superconductivity, *Zh. Eksp. Teor. Fiz. (USSR)* **20** (1950), 1064–1082; Engl. transl. in D. ter Haar, *L. D. Landau; Men of Physics*, Vol. I, Pergamon Press, Oxford, 1965, pp. 138–167.
- [2] M. TINKHAM, *Introduction to Superconductivity* (2nd edition), McGraw-Hill, Inc., New York, 1996.
- [3] A. SCHMID, A time dependent Ginzburg–Landau equation and its application to a problem of resistivity in the mixed state, *Phys. kondens. Materie*, **5** (1966), 302–317.
- [4] L. P. GOR’KOV AND G. M. ÉLIASHBERG, Generalizations of the Ginzburg–Landau equations for non-stationary problems in the case of alloys with paramagnetic impurities, *Zh. Eksp. Teor. Fiz.*, **54** (1968), 612–626; *Soviet Phys.—JETP*, **27** (1968), 328–334.
- [5] Q. DU, M. D. GUNZBURGER, AND J. S. PETERSON, Analysis and approximation of the Ginzburg–Landau model of superconductivity, *SIAM Review*, **34** (1992), 54–81.
- [6] J. FLECKINGER–PELLÉ, H. G. KAPER, AND P. TAKÁČ, Dynamics of the Ginzburg-Landau Equations of Superconductivity, *Nonlinear Anal. — Theory, Methods & Applic.* **32** (1998), 647–665.
- [7] D. W. BRAUN ET AL., Structure of a moving vortex lattice, *Phys. Rev. Lett.*, **76** (1996), 831–834.
- [8] G. W. CRABTREE ET AL., Time-dependent Ginzburg-Landau simulations of vortex guidance by twin boundaries, *Physica C*, **263** (1996), 401–408.
- [9] G. C. CRABTREE ET AL., Numerical simulations of driven vortex systems, Preprint ANL/MCS-P764-0699, Argonne National Laboratory, Argonne, Ill., 1999.
- [10] W. D. GROPP ET AL., Numerical simulations of vortex dynamics in type-II superconductors, *J. Comp. Phys.*, **123** (1996), 254–266.
- [11] N. GALBREATH ET AL., Parallel solution of the three-dimensional, time-dependent Ginzburg-Landau equation, *Proc. Sixth SIAM Conference on Parallel Processing for Scientific Computing*, R. F. Sincovec, D. E. Keyes, M. R. Leuze, L. R. Petzold, and D. A. Reed (eds.), SIAM, Philadelphia, 1993, pp. 160–164.
- [12] J. DONGARRA ET AL., *MPI—The Complete Reference*, Vols. I & II, MIT Press, Cambridge, Mass., 1998.
- [13] W. GROPP ET AL., A High-Performance, Portable Implementation of the MPI Message Passing Interface Standard, Technical Report ANL/MCS-P567-0296, Argonne National Laboratory, Argonne, Ill., 1996.
- [14] J. DOUGLAS AND J. E. GUNN, A general formulation of alternating direction methods—Part I: Parabolic and hyperbolic problems, *Numerische Mathematik*, **6** (1964), 428–453.
- [15] H. G. KAPER AND H. NORDBORO, The frozen-field approximation and the Ginzburg–Landau equations of superconductivity, *J. Engin. Mathematics (to appear)*.